



Article

# Thermodynamic and environmental performance of a Kalina-based multigeneration cycle with biomass ancillary firing for power, water and hydrogen production

Fidelis I. Abam<sup>1\*</sup>, Victor Umeh<sup>2</sup>, Ekwe Bassey Ekwe<sup>3</sup>, Samuel O. Effiom<sup>4</sup>, Jerome Egbe<sup>5</sup>, Adie J. Anyandi<sup>4</sup>, James Enyia<sup>4</sup>, Ugwu Hyginus Ubauike<sup>2</sup>, Macmanus C. Ndukwu<sup>6</sup>

<sup>1</sup>Energy, Exergy and Environment Research Group (EEERG), Department of Mechanical Engineering, University of Calabar, Nigeria

<sup>2</sup>Department of Mechanical Engineering, Michael Okpara University of Agriculture Umudike, Nigeria

<sup>3</sup>Department of Mechanical Engineering, Covenant University Ota, Nigeria

<sup>4</sup>Department of Mechanical Engineering University of Cross River State, Calabar, Nigeria

<sup>5</sup>Department of Civil and Environmental Engineering, University of Cross River State, Calabar, Nigeria

<sup>6</sup>Department of Agricultural and Bioresources Engineering, Michael Okpara University of Agriculture Umudike, Nigeria

## ARTICLE INFO

### Article history:

Received 19 April 2023

Received in revised form

02 June 2023

Accepted 20 June 2023

### Keywords:

Energy, Exergy, Kalina cycle, Sustainability, Hydrogen

\*Corresponding author

Email address:

[fidelisabam@unical.edu.ng](mailto:fidelisabam@unical.edu.ng)

DOI: 10.55670/fpll.futech.3.1.5

## ABSTRACT

The performance of a Kalina-based multigeneration cycle for power, water, and hydrogen production is investigated from thermo-environmental, sustainability, and thermo-economic perspectives. The plant comprises a gas turbine (GT), Kalina cycle (KC), and vapor absorption system (VAS) as the bottoming cycle and an integrated domestic water heater and proton-electron membrane (PEM) electrolyzer for hydrogen production. The system's models were simulated with Engineering Equation Solver (EES) codes. The results indicate a net energy efficiency of 53.48% and exergy efficiencies of 50.05 %, with an additional 30,178 kW of products from the bottoming cycles. The GT contributed approximately 85.81 % of the overall exergy destruction. The system's exergo-thermal index (ETI) stood at 1.713, with the GT only having an ETI of 2.106. Similarly, the exergetic sustainability index (ESI) of the multigeneration plant was not greater than 2.04. The exergoeconomic analysis shows a low average energy cost from the GT, estimated at 0.836 \$/GJ, compared to the Kalina subsystem, which stood at 6.53 \$/GJ. The thermodynamic and cost evaluation of the system demonstrates substantial benefits from the plant, which kept the hydrogen production rate at 0.1524 kg/hr.

## 1. Introduction

The role of energy availability in economic development cannot be over-emphasized. Energy remains the fulcrum for sustainable development [1]. For the past decades, the fundamental processes for energy generation, especially electricity, have been from burning fossil fuels in gas turbine plants, steam plants, and a combination of the two in cogeneration [2, 3]. Several plant configurations have been developed and implemented to increase these thermal plants' energy efficiency. Research is increasing to produce different products from these systems, which has increased in scope in

recent times [4, 5]. However, the configuration of the lower bottoming cycles and the choice of operating parameters play vital roles in developing sustainable products with minimal exergy destruction and environmental impact. Among the many options for lower bottoming cycles to increase energy conversion system products are the organic Rankine cycle (ORC) [6-8], Kalina cycle [9, 10], Goswami cycle [11] steam turbine cycle [12], and for water electrolyzers [13]. Multigeneration plants have been presented in the literature. For example, Dev and Attri [12] presented a Multi-plant cycle based on ORC, which produces six products: electricity,

heating, hot water, hydrogen, cooling, and dry air. The results indicate an energetic coefficient of performance (COP) of approximately 60%, while that for the exergetic COP was estimated at 10%. Similarly, the study in reference [13] presented a primary Brayton cycle with several strings of bottoming cycles that can provide electrical power, domestic water heating, and cooling through refrigeration processes embedded in ORC and vapor absorption cycles. The study obtained energy and exergy efficiencies of 44.22 and 61.50 %, respectively, with an exergo thermal index of 0.675. Additionally, other lower cycles are reported to produce hydrogen, while some are used for the desalination of water [14, 15]. The study in [14] proposed a multi-cycle power plant for cooling, heating, and desalting water production. The result shows that the water production rate was 0.364 kg/s with a cooling rate and power output estimated at 1 MW and 30.5 MW, respectively. Similarly, Abam et al. [15] designed and developed a novel incorporated cycle based on the solid-oxide fuel cell-GT for concurrent fresh water, electricity, and hydrogen production. The exergetic efficiency was estimated at 54.2 % at refresh water rate production of 90.1 m<sup>3</sup>/h at a unit cost of 32.9 \$/GJ. Furthermore, Anvari et al. [16] analyzed an innovative solar-based multigeneration plant. The system was developed for power generation, desalination, and hydrogen production. The thermodynamic assessment indicates that the multigeneration system had 23.2 % as energy efficiency and 6.2% for exergy efficiency. Ref [17] performed a thermodynamic and economic evaluation of a geothermal-based integrated plant which comprises ORC, domestic water heater, electrolyzer, and absorption refrigeration system to produce hydrogen and electricity, heating and cooling. The total efficiencies were estimated at 34.98% energy and 49.17% exergy, whereas the hydrogen production rate and unit cost of production stood at 0.052 g/s and 5.967 \$/kg, respectively. Furthermore, Khalid et al. [18] presented a techno-economic valuation of a solar, geothermal-driven multigeneration system to produce; electricity cooling, hot water, heating, and hydrogen. The hydrogen production rate was estimated at 2.7 kg/h while \$ 476,000 and \$ 0.089/kWh were the net presents and the levelized cost of electricity. Ref [19] proposed a geothermal multigeneration plant comprising an electrolyzer, absorption cycle, Kalina, and flash cycles for hydrogen and ice production. The results show a maximum exergy efficiency of 26.25%. Multigeneration systems require adding bottoming cycles to gas-fired, geothermal, or solar-based topping cycles to generate multiple products. Thus, several choices on the mode of a bottoming cycle depend on several factors. These may include the exiting temperature of the topping cycle flue gas, the required efficiency, the quantity of desired products, and the economic and environmental impact of the bottoming cycle. The Kalina cycle can provide an efficiency gain of 10-50 % compared to the conventional thermodynamic cycles with equivalent output. However, system modification or adjustment in the thermodynamic pathways may be necessary to maximize the waste heat used in the bottoming cycles. The current study introduced a dual heat input to improve the thermal heat requirement of the PEM electrolyzer from the same energy source. The latter will increase the hydrogen production yield since hydrogen production yield is related to the quantity of electricity and heat in the PEM electrolyzer. An external thermal heat source for the electrolyzer may increase system costs and maintenance procedures. In the current study, an external heat source for the electrolyzer was avoided. The system was designed to utilize the dual heat input from the condensate of

the two Kalina condensers. The latter innovation improved the hydrogen production yield and reduced the multigeneration plant's economic cost. In light of this development, this research proposes a modified Kalina-based multigeneration cycle incorporating biomass gasification for reheating in the combined topping cycle. The study thus determines the thermo-environmental and thermo-economic performance of the modified Kalina-based multigeneration cycle. The best operating parameters corresponding to low operating costs and environmental impact were equally evaluated.

## 2. System description

The operation starts at state (1) in Figure 1, where the air is drawn to the low-pressure compressor (LPC), and the temperature and pressure are raised to state (2). An intercooler reduces the mechanical work required for compression from the state (2) to (3). The cooled air is recompressed by a high-pressure compressor (HPC) at state (3). The compressed air is heated partly by an expanded gas from the low-pressure turbine (LPT). Fuel is added to the combustion chamber (CC) at constant pressure, raising the energy level of the air stream to the high-pressure turbine (HPT), which expands to a pressure sufficient to drive both the HPC and LPC. The expanded gas is reheated with biomass gas for expansion in the LPT to produce shaft work which drives an alternator to produce electricity. After partly raising the air temperature in a heat exchanger, the expanded gas is made to pass through a vapor generator which powers the Kalina cycle embedded with a vapor absorption system (VAS). Ammonium water and lithium bromide drive the Kalina and VAS system, respectively. In the Kalina cycle, after the ammonia water solution receives heat, the energy level of the mixture increases at the state (17). The separator is provided to separate the ammonium water solution into rich and weak solutions. The rich solution expands in the turbine producing electrical energy. The expanded vapor, still rich, is further separated in another separating vessel. The rich part of the mixture is condensed and throttled, and evaporated, providing cooling in the first part of this cycle. Meanwhile, the weak solution already expanded in the turbine and separated is throttled to a pressure equal to the weak solution at state (24) and mixes with the hot vapor leaving at state (23) after being equally throttled. These two streams heat the desorber for powering the VAS. The exiting stream at the desorber is passed through a heat exchanger before being added up with the resulting stream used for refrigeration at state (31). The summation produces a stream at state (32), which passes through a heat exchanger and condenser and is finally pumped to the vapor generator to commence the next cycle. The heat obtained from the dual condensation of the expanded refrigerants in the Kalina cycle is used to heat the water directed for electrolysis in the PEM electrolyzer. Part of the electricity generated from the Kalina turbine is utilized for the electrolyser's operation to produce hydrogen.

## 3. Methodology and system modelling

### 3.1 Thermodynamic modelling

The general energy flow balances in a thermodynamic system under steady for the  $k^{th}$  component are presented in Eq (1) [20, 21].



$$\dot{C}_j = c_j \dot{E}x_j \quad (7)$$

$$\dot{C}_{w,k} = c_w \dot{W} \quad (8)$$

$$\dot{C}_{q,k} = c_q \dot{Q} \quad (9)$$

The cost rate  $\dot{Z}_k$  for the components is present as:

$$\dot{Z}_k = \frac{PECF \times CRF \times \phi}{N \times 3600} \quad (10)$$

PECF, CRF, and  $\phi$  represent the purchase of equipment cost function, capital recovery factor, and maintenance factor, respectively. The system's annual operational hours are denoted with N while the capital recovery factor is expressed:

$$CRF = \frac{i|1+i|^n}{|1+i|^n - 1} \quad (11)$$

Where  $n$  is the estimated plant life in years, another exergy-related index is the cost of exergy of product and fuel for the component. A detailed description of the component cost of fuel and product is found in [22]. The general relationship for evaluating the specific cost of a product for the  $k^{\text{th}}$  component  $c_{P,k}$  (\$/kJ), and that of fuel  $c_{F,k}$  (\$/kJ), as well as the exergoeconomic factor,  $f$  is presented in Eqs (12) – (14), respectively.

$$c_{P,k} (\$/kJ) = \frac{\dot{C}_{P,k}}{\dot{E}_{P,k}} \quad (12)$$

$$c_{F,k} (\$/kJ) = \frac{\dot{C}_{F,k}}{\dot{E}_{F,k}} \quad (13)$$

$$f = \frac{\dot{Z}_k}{\dot{Z}_k + \dot{C}_{D,k}} \quad (14)$$

The cost of exergy destruction is expressed in Eq (15). A summary of the cost-related terms for Figure 1 is presented in Table 2, while the PEC for the plant components is shown in Table 3.

$$\dot{C}_{D,k} = c_{P,k} E_{D,k} \quad (15)$$

### 3.2 Thermoenvironmental analysis

The environmental effect is evaluated by approximating the measure of pollutants produced by the plant. These include nitrogen oxide,  $\dot{m}_{NO_x}$  (kg/s),  $CO_2$ ,  $\dot{m}_{CO_2}$  (kg/s) and CO,  $\dot{m}_{CO}$  (kg/s). The quantity of these emissions produced and their production rates depend on the following indices: retention time,  $\tau$  (s), combustion chamber pressure drop,  $\Delta P_{CC}$  (kPa), adiabatic flame temperature,  $T_{pz}$  presented [23, 24]. Consequently, the emission rates of production and the harmful emission factor  $F_{EF}$ , are defined in Eqs (16) to (20).

$$\dot{m}_{NO_x} = \frac{1.5 \times 10^{15} \tau^{0.5} e^{-(7110/T_{pz})}}{P_6^{0.05} \left(\frac{\Delta P_{CC}}{P_6}\right)^{0.5}} \quad (16)$$

$$\dot{m}_{CO} = \frac{1.79 \times 10^8 \tau^{0.5} e^{(7800/T_{pz})}}{P_6^{0.05} \tau \left(\frac{\Delta P_{CC}}{P_6}\right)^{0.5}} \quad (17)$$

$$\dot{m}_{CO_2} = yCO_2 \dot{m}_g \left(\frac{\bar{M}_{CO_2}}{\bar{m}_g}\right) \quad (18)$$

$$CO_{2,sp} = 3600 \left(\frac{\dot{m}_{CO_2}}{\dot{W}_{net}}\right) \quad (19)$$

$$F_{EF} = \frac{\dot{m}_{NO_x} + \dot{m}_{CO} + \dot{m}_{CO_2}}{\dot{m}_g} \quad (20)$$

Where  $CO_{2,sp}$  ( $kg_{CO_2}/MWh$ ) describes the amount and the specific  $CO_2$  emissions. Similarly,  $\dot{m}_g$ ,  $\bar{M}$ ,  $yCO_2$  and  $\bar{M}_{CO_2}$  are

the rate of mass flow of flue gas, flue gas molar mass, mass fraction and the  $CO_2$  molar mass. The adiabatic flame temperature  $T_{pz}$  is defined by Eq (21). All parameters, constants and the terms  $x$ ,  $y$  and  $z$  in Eq (21) are estimated according to the procedure in [24].

$$T_{pz} = A \sigma^\alpha \exp[\beta(\sigma + \lambda)^2] \pi^{x^*} \theta^{y^*} \psi^{z^*} \quad (21)$$

### 3.3 Sustainability indicator

#### 3.3.1 The exergetic utility index

The exergetic utility index (EUI) is depicted in Eq (22) and measures the extent of exergy resource utilization in a system regarding the same system's net output. It is a function of combustion efficiency,  $\lambda_{CC}$ , net output,  $\dot{W}_{net}$ , exergy input,  $\dot{E}_{xin}$  and the exergy efflux to the environment,  $\dot{E}_{xout}$  [15].

$$EUI = \frac{\lambda_{CC} \times \dot{W}_{net}}{\dot{E}_{xin} - \dot{E}_{xout}} \quad (22)$$

#### 3.3.2 Exergo-thermal index

The exergo-thermal index (ETI) measures the thermal impact of the system on the environment during the energy conversion process. Low values of ETI are desired and can be achieved by continuously utilizing high-temperature flue gas from energy conversion systems in powering other low-heat bottoming cycles, expressed as:

$$ETI = \frac{EUI}{\gamma} = \frac{\lambda_{CC} \times \dot{W}_{net}}{(\dot{E}_{xin} - \dot{E}_{xout})} \times \frac{1}{\gamma} \quad (23)$$

Where  $\gamma$  denotes the enviro-thermal conservation factor, expressed as:

$$\gamma = \frac{T_0}{T_f} \quad (24)$$

Where  $T_0$  is the ambient temperature and  $T_f$  is the temperature of the flue gas.

#### 3.3.3 Exergetic sustainability index

The exergetic sustainability index (ESI) compares the magnitudes of a system's net product to its exergy destruction. A system with ESI less than unity underutilizes the exergy resources, and it is not desirable. Conversely, a system with ESI greater than unity is desirable as its net output exceeds the total exergy destruction. The ESI is expressed by [25].

$$ESI = \frac{\dot{W}_{Net}}{\dot{E}_{D,Total}} \quad (25)$$

## 4. Results and discussion

### 4.1 Thermodynamic properties and operating conditions

The simulation results of the system were obtained using a developed computer code written in EES. The initial operating conditions are presented in Table 4. The model development was built on the succeeding assumptions: the surrounding temperature and pressure exist at 25 °C and 1.013 bar, respectively. The system and its subcomponents were evaluated at steady-state conditions. Pressure and temperature variations were neglected. The system's boundaries were treated as adiabatic. The working fluid for the Kalina system is ammonium water solution at 0.28. Likewise, the properties of the system, including the enthalpy and exergy flow rates used to calculate system performance, are shown in Table 5.

**Table 2.** Component cost and auxiliary equations for the multigeneration plant

Component	Exergoeconomic balance	Auxiliary equation
GT LPC	$\dot{C}_1 + \dot{C}_{W_{LPC}} + \dot{Z}_{LPC} = \dot{C}_2$	Nil
GT intercooler	$\dot{C}_2 + \dot{C}_{48} + \dot{Z}_{INT} = \dot{C}_3 + \dot{C}_{49}$	$\dot{C}_2 \dot{E}_3 - \dot{C}_3 E_2 = 0$
GT HPC	$\dot{C}_3 + \dot{C}_{W_{HPC}} + \dot{Z}_{HPC} = \dot{C}_4$	Nil
GT Hex	$\dot{C}_4 + \dot{C}_{11} + \dot{Z}_{HEX} = \dot{C}_5 + \dot{C}_{12}$	$\dot{C}_{11} \dot{E}_{12} - \dot{C}_{12} E_{11} = 0$
GT CC	$\dot{C}_5 + \dot{C}_6 + \dot{Z}_{CC} = \dot{C}_7$	Nil
GT HPT	$\dot{C}_7 + \dot{Z}_{HPT} = \dot{C}_8 + \dot{C}_{W_{HPC}} + \dot{C}_{W_{LPC}}$	$\dot{C}_7 \dot{E}_8 - \dot{C}_8 E_7 = 0$ $\dot{C}_{W_{LPC}} \dot{W}_{HPC} - \dot{C}_{W_{HPC}} \dot{W}_{LPC} = 0$
GT REH	$\dot{C}_8 + \dot{C}_9 + \dot{Z}_{HPT} = \dot{C}_{10}$	Nil
GT LPT	$\dot{C}_{10} + \dot{Z}_{LPT} = \dot{C}_{11} + \dot{C}_{W_{LPT}}$	$\dot{C}_{10} \dot{E}_{11} - \dot{C}_{11} E_{10} = 0$
Kal. Vap Gen.	$\dot{C}_{12} + \dot{C}_{37} + \dot{Z}_{VG} = \dot{C}_{13} + \dot{C}_{17}$	$\dot{C}_{12} \dot{E}_{13} - \dot{C}_{13} E_{12} = 0$
Kal. Sep 1	$\dot{C}_{17} + \dot{Z}_{SEP1} = \dot{C}_{18} + \dot{C}_{22}$	$\dot{C}_{18} \dot{E}_{22} - \dot{C}_{22} E_{18} = 0$
Kal. Valve 1	$\dot{C}_{22} + \dot{Z}_{V1} = \dot{C}_{23}$	Nil
Kal. Valve 2	$\dot{C}_{21} + \dot{Z}_{V2} = \dot{C}_{24}$	Nil
Kal. Turb.	$\dot{C}_{18} + Z_{KalTurb} = \dot{C}_{20} + \dot{C}_{W_{KalTurb}} + \dot{C}_{W_{Pump1}}$	$\dot{C}_{18} \dot{E}_{20} - \dot{C}_{20} E_{18} = 0$ $\dot{C}_{W_{KalTurb}} \dot{W}_{Pump1} - \dot{C}_{W_{Pump1}} \dot{W}_{KalTurb} = 0$
Kal. Sep 2	$\dot{C}_{20} + \dot{Z}_{SEP2} = \dot{C}_{21} + \dot{C}_{28}$	$\dot{C}_{21} \dot{E}_{28} - \dot{C}_{28} E_{21} = 0$
Kal. CND 1	$\dot{C}_{28} + \dot{C}_{59} + \dot{Z}_{CND1} = \dot{C}_{29} + \dot{C}_{60}$	$\dot{C}_{28} \dot{E}_{29} - \dot{C}_{29} E_{28} = 0$
Kal. Valve 3	$\dot{C}_{29} + \dot{Z}_{V3} = \dot{C}_{30}$	Nil
Kal. Evap 1	$\dot{C}_{30} + \dot{C}_{67} + \dot{Z}_{EVP} = \dot{C}_{31} + \dot{C}_{68}$	$\dot{C}_{67} \dot{E}_{68} - \dot{C}_{68} E_{67} = 0$
Kal. HEX 1	$\dot{C}_{26} + \dot{C}_{36} + \dot{Z}_{HEX} = \dot{C}_{27} + \dot{C}_{37}$	$\dot{C}_{26} \dot{E}_{27} - \dot{C}_{27} E_{26} = 0$
Kal. HEX 2	$\dot{C}_{32} + \dot{C}_{35} + \dot{Z}_{HEX} = \dot{C}_{33} + \dot{C}_{36}$	$\dot{C}_{32} \dot{E}_{33} - \dot{C}_{33} E_{32} = 0$
Kal. CND 2	$\dot{C}_{33} + \dot{C}_{57} + \dot{Z}_{CND2} = \dot{C}_{34} + \dot{C}_{58}$	$\dot{C}_{33} \dot{E}_{34} - \dot{C}_{34} E_{33} = 0$
Kal. Pump 1	$\dot{C}_{34} + \dot{C}_{W_{Pump1}} + Z_{Pump1} = \dot{C}_{35}$	Nil
VAS desorber	$\dot{C}_{25} + \dot{C}_{44} + \dot{Z}_{DESB} = \dot{C}_{26} + \dot{C}_{38} + \dot{C}_{45}$	$\dot{C}_{25} \dot{E}_{26} - \dot{C}_{26} E_{25} = 0$ $\dot{C}_{38} \dot{E}_{45} - \dot{C}_{45} E_{38} = 0$ $\dot{C}_{45} \dot{E}_{46} - \dot{C}_{46} E_{45} = 0$
VAS HEX 3	$\dot{C}_{43} + \dot{C}_{45} + \dot{Z}_{HEX} = \dot{C}_{44} + \dot{C}_{46}$	$\dot{C}_{45} \dot{E}_{46} - \dot{C}_{46} E_{45} = 0$
VAS Valve 4	$\dot{C}_{39} + \dot{Z}_{V4} = \dot{C}_{40}$	Nil
VAS Pump 2	$\dot{C}_{42} + \dot{C}_{W_{Pump2}} + \dot{Z}_{Pump2} = \dot{C}_{43}$	Nil
VAS Absorber	$\dot{C}_{41} + \dot{C}_{47} + \dot{C}_{65} + \dot{Z}_{ABS} = \dot{C}_{42} + \dot{C}_{66}$	$ \dot{C}_{66} - \dot{C}_{65}  * \dot{E}_{42} - \dot{C}_{42} *  \dot{E}_{66} - \dot{E}_{65}  = 0$
VAS EVP 2	$\dot{C}_{40} + \dot{C}_{63} + \dot{Z}_{EVP} = \dot{C}_{41} + \dot{C}_{64}$	$\dot{C}_{63} \dot{E}_{64} - \dot{C}_{64} E_{63} = 0$
VAS Valve 5	$\dot{C}_{46} + \dot{Z}_{V5} = \dot{C}_{47}$	Nil
VAS CND 3	$\dot{C}_{38} + \dot{C}_{61} + \dot{Z}_{CND3} = \dot{C}_{39} + \dot{C}_{62}$	$\dot{C}_{38} \dot{E}_{39} - \dot{C}_{39} E_{38} = 0$
Water heater	$\dot{C}_{13} + \dot{C}_{15} + \dot{Z}_{WH} = \dot{C}_{14} + \dot{C}_{16}$	$\dot{C}_{13} \dot{E}_{14} - \dot{C}_{14} E_{13} = 0$
PEM Electrolyser	$\dot{C}_{52} + \dot{C}_{19} + \dot{Z}_{ELECTR.} = \dot{C}_{53} + \dot{C}_{54}$	$ \dot{C}_{52} + \dot{C}_{19}   \dot{E}_{53} + \dot{E}_{54}  -  \dot{C}_{53} + \dot{C}_{54}   \dot{E}_{52} + \dot{E}_{19}  = 0$
PEM Hex	$\dot{C}_{58} + \dot{C}_{60} + \dot{C}_{50} + \dot{Z}_{HEX} = \dot{C}_{51} + \dot{C}_{69}$	$ \dot{C}_{58} + \dot{C}_{60}  * \dot{E}_{69} - \dot{C}_{69} *  \dot{E}_{58} + \dot{E}_{60}  = 0$
PEM O <sub>2</sub> separator	$\dot{C}_{54} + \dot{Z}_{Oxygensep} = \dot{C}_{55} + \dot{C}_{56}$	$\dot{C}_{55} \dot{E}_{56} - \dot{C}_{56} E_{55} = 0$

**4.2 Performance analysis of the system based on operating data**

The performance indices considered for the study are presented in Table 6. The system net energy and exergy efficiency was calculated at 53.48 and 50.05 %, respectively. The multigeneration system improved the topping cycle by 19.03 and 2.58 % in energy and exergy efficiencies, respectively. The improvement was ascribed to the added products from the bottoming cycles estimated at 30,178 kW. These additional products include the power generated from the Kalina turbine, VAS and Kalina system cooling, and the quantity of hot water produced from the domestic water heater. The net power from the topping cycle stood at 55.605 MW. Also, the system hydrogen production rate stood at 0.1524 kg/h, with about 3498 kW of cooling and a coefficient of performance of 4.304.

**4.3 Component exergy destruction (ED) rates**

The system components' ED rates are shown in Table 7. About 85.81 % of EDs were from the GT topping cycle due to significant ED rates around the combustion chamber (CC). The GT CC and reheater contributed approximately 54.65 and 22.57 % of the ED, respectively, to the total ED. The main reason for the large ED in the CC is the large temperature

difference between the combustion gases and the hot air. Using alternative preheated fuels before combustion will reduce ED in the CC. In the present study, operating the reheater with biomass syngas at 154 °C reduced ED by nearly 25 %. Furthermore, with the integration of the bottoming cycles, about 15089.77 kW ED was avoided, equivalent to 14.19 % of the total ED. Also, an additional product of 30178 kW was achieved, which increased the exergetic sustainability of the bottoming cycle to approximately 1.99. The latter validates retrofitting the topping cycle, the Kalina and VAS cycles.

**4.4 Exergoeconomic parameters of the plant**

The values of the initial investment, monetary flow rate and levelized capital cost (LECC) rate are shown in Table 8. The GT HPT has the highest levelized cost per hour, calculated at 41.5 \$/hr, followed by GT LPT and GT LPC, estimated at 34.19 and 12.17 \$/hr, respectively. Similarly, the exergoeconomic parameters of the subsystems are depicted in Tables 9-12. From Table 9, the combustion chamber and reheater contribute about 39.903 and 20.613 \$/hr to the total ED cost calculated at 106.4 \$.hr. The CC and reheater have the least exergoeconomic factors of 0.112 and 0.279, respectively. One method to reduce ED cost in the CC is to improve combustion efficiency and reduce the temperature difference

between the working fluid and combustion fuel. However, this can be achieved by firing the CC with preheated fuel. In the Kalina subsystem (Table 10), the vapour generator (VG) cost improvement potential is primarily dependent on the equipment cost rates than the cost due to ED.

Subsequently, since the VG cost is directly linked to the quantity of heat transfer, the choice of working fluid and efficient design of the heat transfer area is germane in reducing the cost of the system components.

**Table 3.** Component cost functions, cost of product and cost of fuel [15, 18, 22]

Component	Cost function [\$]	Cost of product	Cost of fuel
GT LPC	$\frac{39.5\dot{m}_2}{0.9 - \eta_{LPC}} \left  \frac{P_2}{P_1} \right  \ln \left  \frac{P_2}{P_1} \right $	$\dot{C}_2 - \dot{C}_1$	$x \cdot \dot{W}_{HPT}$
GT intercooler	$130 \left  \frac{A_{INT}}{0.093} \right ^{0.78}$	$\dot{C}_{49} - \dot{C}_{48}$	$\dot{C}_2 - \dot{C}_3$
GT HPC	$\frac{39.5\dot{m}_4}{0.9 - \eta_{HPC}} \left  \frac{P_4}{P_3} \right  \ln \left  \frac{P_4}{P_3} \right $	$\dot{C}_4 - \dot{C}_3$	$[1 - x] \cdot \dot{W}_{HPT}$
GT Hex	$130 \left  \frac{A_{HEX}}{0.093} \right ^{0.78}$	$\dot{C}_5 - \dot{C}_4$	$\dot{C}_{11} - \dot{C}_{12}$
GT CC	$\left  \frac{46.08\dot{m}_5}{0.995 - \frac{P_7}{P_5}} \right  [1 + \exp(0.018T_7 - 26.4)]$	$\dot{C}_7$	$\dot{C}_5 + \dot{C}_6$
GT HPT	$\left  \frac{479.34\dot{m}_7}{0.92 - \eta_{HPT}} \right  \ln \left  \frac{P_7}{P_8} \right  [1 + \exp[0.036T_7 - 54.4]]$	$\dot{W}_{HPT}$	$\dot{C}_7 - \dot{C}_8$
GT REH	$\left  \frac{46.08\dot{m}_8}{0.995 - \frac{P_{10}}{P_8}} \right  [1 + \exp(0.018T_{10} - 26.4)]$	$\dot{C}_{10}$	$\dot{C}_8 + \dot{C}_9$
GT LPT	$\left  \frac{479.34\dot{m}_7}{0.92 - \eta_{LPT}} \right  \ln \left  \frac{P_{10}}{P_{11}} \right  [1 + \exp[0.036T_{10} - 54.4]]$	$\dot{W}_{LPT}$	$\dot{C}_{10} - \dot{C}_{11}$
Kal. Vap Gen.	$130 \left  \frac{A_{VASEN}}{0.093} \right ^{0.78}$	$\dot{C}_{17} - \dot{C}_{37}$	$\dot{C}_{12} - \dot{C}_{13}$
Kal. Valve 1	$37 \left  \frac{P_{22}}{P_{23}} \right ^{0.68}$	$\dot{C}_{23}$	$\dot{C}_{22}$
Kal. Valve 2	$37 \left  \frac{P_{21}}{P_{24}} \right ^{0.68}$	$\dot{C}_{24}$	$\dot{C}_{21}$
Kal. Turb.	$\left  \frac{479.34\dot{m}_{32}}{0.92 - \eta_T} \right  \ln \left  \frac{P_{18}}{P_{20}} \right  [1 + \exp[0.036T_{18} - 54.4]]$	$\dot{W}_{LPT} + \dot{W}_{KalP_1} + \dot{W}_{VASP_2}$	$\dot{C}_{18} - \dot{C}_{20}$
Kal. CND 1	$516.62 \frac{\dot{Q}_{KalCND1}}{0.15\Delta T_{KalCND1}}$	$\dot{C}_{60} - \dot{C}_{59}$	$\dot{C}_{28} - \dot{C}_{29}$
Kal. Valve 3	$37 \left  \frac{P_{29}}{P_{30}} \right ^{0.68}$	$\dot{C}_{30}$	$\dot{C}_{29}$
Kal. Evap 1	$309.4 \left  \frac{\dot{Q}_{KalEVP1}}{0.15\Delta T_{KalEVP1}} \right ^{0.85}$	$\dot{C}_{31} - \dot{C}_{30}$	$\dot{C}_{67} - \dot{C}_{68}$
Kal. HEX 1	$130 \left  \frac{A_{KalHEX1}}{0.093} \right ^{0.78}$	$\dot{C}_{37} - \dot{C}_{36}$	$\dot{C}_{25} - \dot{C}_{26}$
Kal. CND 2	$516.62 \frac{\dot{Q}_{KalCND2}}{0.15\Delta T_{KalCND2}}$	$\dot{C}_{58} - \dot{C}_{57}$	$\dot{C}_{33} - \dot{C}_{34}$
Kal. Pump 1	$705.5 \left  0.001W_{KalPump1} \right ^{0.71} \left  1 + \frac{0.2}{1 - \eta_P} \right $	$\dot{C}_{35} - \dot{C}_{34}$	$W_{KalP_1}$
VAS HEX 3	$130 \left  \frac{A_{VASEX3}}{0.093} \right ^{0.78}$	$\dot{C}_{44} - \dot{C}_{43}$	$\dot{C}_{45} - \dot{C}_{46}$
VAS Valve 4	$37 \left  \frac{P_{39}}{P_{40}} \right ^{0.68}$	$\dot{C}_{47}$	$\dot{C}_{46}$
VAS Pump 2	$705.5 \left  0.001W_{KalPump2} \right ^{0.71} \left  1 + \frac{0.2}{1 - \eta_P} \right $	$\dot{C}_{43} - \dot{C}_{42}$	$W_{VASP_2}$
VAS EVP 2	$309.4 \left  \frac{\dot{Q}_{VASEVP2}}{0.15\Delta T_{VASEVP2}} \right ^{0.85}$	$\dot{C}_{41} - \dot{C}_{40}$	$\dot{C}_{63} - \dot{C}_{64}$
VAS CND 3	$516.62 \frac{\dot{Q}_{VASCND3}}{0.15\Delta T_{VASCND3}}$	$\dot{C}_{62} - \dot{C}_{61}$	$\dot{C}_{38} - \dot{C}_{39}$
Water heater	$130 \left  \frac{A_{HEATER}}{0.093} \right ^{0.78}$	$\dot{C}_{16} - \dot{C}_{15}$	$\dot{C}_{13} - \dot{C}_{14}$

**Table 4.** Design operating data [15, 23]

Parameter	Unit	Value
Ambient temperature	°C	25
Ambient pressure	Bar	1.013
GT Lower compression ratio	Dim.	3.162
GT Higher compression ratio	Dim.	3.162
Overall pressure ratio	Dim.	10
GT Heat exchanger effectiveness	%	75
Low pressure turbine isentropic efficiency	%	85
High pressure turbine isentropic efficiency	%	85
Low pressure compressor isentropic efficiency	%	80
High pressure compressor isentropic efficiency	%	80
mass of air to the topping cycle	kg/s	200
mass of gas at the inlet to the first combustion chamber	kg/s	3.131
mass of gas at the inlet to the reheater	kg/s	21.49
High pressure turbine inlet temperature	°K	1350
Low pressure turbine inlet temperature	°K	1200
The exit temperature of intercooler water	°C	85

The pump has an exergoeconomic factor of 1, suggesting a zero contribution to ED costs. This is realistic as the system pumps operated in isentropic conditions. The total cost of product and fuel for the GT (Table 9) is calculated at 2.67 and 6.06 \$/GJ, respectively, while that for the Kalina (Table 10) and VAS subsystems (Table 11) exist at 32.92 and 84.89 \$/GJ, and 17.97 and 25.93 \$/GJ, respectively. The results show a lower average energy cost from the GT (0.836 \$/GJ) compared to the Kalina subsystem and the VAS. For the PEM electrolyzer, economic parameters are equally presented in Table 12. Furthermore, the exergoeconomic factors (*fk*) for all the subsystems are similarly presented in Tables 9-12, estimated at 59.59%, 68 %, 8.656%, 30.71%, 47.41% for GT, KAL, VAS, and PEM electrolyzer respectively. Low values of *fk* for any system component indicate high ED cost, which signifies a high prospective for improvement, while high values of relative cost difference (*rk*) indicate prospects for system optimisation. The *rk* for the GT, KAL, VAS, and PEM electrolyzer subsystems are calculated at 127 %, 157 %, 30% and 30.71 %, respectively. The joined effects of *rk* and *fk* show that the GT and KAL subsystems have the highest potential for improvement, followed by VAS and PEM electrolyzer, which have the narrow potential for optimisation.

**4.5 Sensitivity analysis**

**4.5.1 Effect of dead state temperature on system efficiencies**

Figure 2 presents the effect of dead state temperature on system performance. The energy and exergy efficiencies of the GT and Kalina cycles and the coefficient of performance of the VAS were observed. The dead state temperature (DST) ranged between 288 and 302 K. The results show that the DST increase led to a reduction in system efficiency. At high DSTs, the compressor work increases, reducing the net system output, especially at the topping GT cycle. The results also show that for every 5 K rise in DST, the energy and exergy efficiency reduced by 0.40 and 0.44 %, respectively. The COP of the VAS was estimated at 4.30 and is constant throughout the DST range, showing that the DST has no direct link with COP measured parameters.

**4.5.2 Effect of heat input on the PEM electrolyzer heat exchanger**

The effect of the required temperature of heating at the inlet to the PEM heat exchanger (HEX) is investigated on the hydrogen yield rate (Figure 3). The water inlet from the condenser of the Kalina system improves the quantity of the hydrogen production rate due to higher PEM water inlet rate to cater for the high energy exchange required in the HEX. Since the temperature of the water entering the PEM electrolyzer is fixed at 95°C, the figure demonstrates the range of water temperatures at the PEM HEX. At most, 102.02°C is required for optimum hydrogen yield with other operating PEM electrolyzer parameters constant as indicated in its modelling.

**4.5.3 Effect of gasifier temperature on hot water rate power output**

Figure 4 shows the effect of gasifier temperature in the topping cycle on the quantity of hot water production at a given hot water temperature and the magnitude of power in the Kalina turbine. Very high gasifier temperatures result in slightly reduced biomass syngas calorific value. Thus, the energy level of the bottoming cycles, including the water heater, is reduced, affecting the quantity of hot water at 95°C. However, the power output from the Kalina turbine was constant at 181 kW. This is attributable to the fixed operating conditions of the Kalina system within a range of heat transfer requirements around the Kalina vapour generator.

**4.5.4 Effect of ammonia mass fraction on cooling and turbine output**

The effect of ammonia mass fraction on the power output and cooling rate of the Kalina system is presented in Figure 5. In the design condition, a mass fraction of 0.28. The result indicates that increasing ammonium mass fraction leads to a higher turbine work and cooling rate. However, at mass fractions higher than 30 per cent, and with the operating pressures in the system, the pump work requirements are significantly higher than the turbine output. Therefore, it is not feasible to operate the system with an ammonia mass fraction in excess of 0.30.

**Table 5.** Thermodynamic properties at the state points

State	Temperature [°C]	Pressure [Bar]	Enthalpy [kJ/kg]	Entropy [kJ/kg.K]	Mass [kg]	Exergy [kW]
1	25	1.013	298.40	5.695	200	0.00
2	170.1	3.203	445.00	5.765	200	25150.00
3	120	3.203	397.90	5.643	200	22965.00
4	311.3	10.13	590.90	5.72	200	57016.00
5	523.2	10.13	818.10	6.051	200	82706.00
6	25	10.13	42300.00	-	2.533	124996.00
7	977	10.13	1337.00	6.565	202.5	157799.00
8	689.7	2.843	1004.00	6.628	202.5	86580.00
9	427	2.843	19841.00	-	2.991	62661.00
10	927	2.843	1278.00	6.882	205.5	128628.00
11	696.6	1.013	1012.00	6.932	205.5	70840.00
12	484.7	1.013	776.00	6.658	205.5	39178.00
13	471	1.013	761.10	6.638	205.5	37326.00
14	349.6	1.013	631.20	6.448	205.5	22305
15	20	1.013	83.30	0.294	85	0.00
16	95	1.013	397.40	1.248	85	2523.00
17	180	20	1264.00	3.639	2.5	862.60
18	180	20	2164.00	5.901	0.97	606.80
19	-	-	-	-	-	4.774
20	136.9	7	1971.00	5.901	0.97	419.60
21	136.9	7	509.50	1.753	0.0644	4.69
22	180	20	694.10	2.205	1.53	206.70
23	79.8	0.8	694.10	2.39	1.53	122.20
24	77.6	0.8	509.50	1.821	0.0644	3.39
25	79.7	0.8	686.70	2.367	1.594	125.60
26	60	0.8	176.80	0.8905	1.594	14.33
27	55	0.8	146.50	0.799	1.594	9.42
28	136.9	7	2080.00	6.209	0.9056	412.80
29	42.9	7	-42.60	0.48	0.9056	36.90
30	-5.5	0.8	-42.60	0.5609	0.9056	15.08
31	15	0.8	332.40	1.909	0.9056	-9.22
32	43.3	0.8	213.80	1.236	2.5	25.78
33	38	0.8	123.00	0.9479	2.5	13.61
34	25	0.8	-73.38	0.3073	2.5	-0.06
35	25.1	20	-71.24	0.3073	2.5	5.28
36	40	20	-7.27	0.5168	2.5	9.19
37	50	20	35.55	0.6514	2.5	15.91
38	79.7	0.07424	2649.00	8.478	1.5	189.40
39	41	0.07424	171.10	0.5836	1.5	2.20
40	1.7	0.006812	171.10	0.6229	1.5	-15.35
41	1.7	0.006812	2503.00	9.114	1.5	-312.80
42	34.6	0.006812	92.00	0.1987	11.16	3.02
43	34.6	0.006812	92.00	0.1987	11.16	3.02
44	67	0.006812	156.30	0.3978	11.16	58.69
45	79.7	0.006812	229.30	0.4167	9.661	40.51
46	45	0.006812	169.30	0.2361	9.661	-19.08
47	35	0.006812	169.30	0.1817	9.661	137.40
48	20	1.013	83.30	0.294	37.58	0.00
49	80	1.013	334.30	1.073	37.58	705.30
50	20	1.013	83.30	0.294	5	0.00
51	95	1.013	397.40	1.248	5	148.40
52	85	1.013	355.30	1.132	10	221.60
53	85	1.013	4843.00	56.17	0.0000423	0.00
54	85	1.013	355.30	1.132	5	110.80
55	85	1.013	55.01	0.1683	0.000336	0.00
56	85	1.013	355.30	1.132	5	110.80
57	20	1.013	83.30	0.294	8.383	0.00
58	34	1.013	141.90	0.4893	8.383	3.18
59	20	1.013	83.30	0.294	7.065	0.00
60	85	1.013	355.30	1.132	7.065	156.60
61	20	1.013	83.30	0.294	44.42	0.00
62	40	1.013	166.96	0.5702	44.42	59.99
63	25	1.013	298.42	5.695	151.5	0.00
64	2	1.013	275.30	5.614	151.5	142.40
65	20	1.013	83.30	0.294	69.55	0.00
66	35	1.013	146.00	0.5029	69.55	35.41
67	25	1.013	298.40	5.695	13.01	0.00
68	-1	1.013	272.30	5.603	13.01	15.73
69	33	1.013	137.80	0.4762	15.45	4.14

**Table 6.** Performance parameters of the energy system

Performance Index	Unit	Value
LPC Power	MW	29.151
HPC Power	MW	38.743
LPT Power	MW	55.605
HPT Power	MW	68.754
GT Net Power Output	MW	55.605
GT Relative Exergy Efficiency	%	29.63
Kalina Relative Exergy Efficiency	%	11.13
Kalina Relative Energy Efficiency	%	16.97
VAS COP	-	4.304
Kalina turbine power	kW	187.2
Kalina pump power	kW	5.337
Kalina evaporator cooling	kW	339.6
Kalina Exergy of cooling	kW	24.3
Kalina net power	kW	181.9
VAS evaporator cooling	kW	3498
Exergy of cooling	kW	297.4
VAS desorber heat	kW	812.9
PEM hydrogen output	kg/h	0.1524
System net output	MW	86.320
System net input	MW	161.403
System net energy efficiency	%	53.48
System net exergy efficiency	%	50.05

**4.5.5 Gasifier mass flow rate on thermo environmental parameters and hot water production rate**

The effect of the gasifier mass flow rate at the reheater was investigated on the quantity of hot water production and thermo-environmental parameters, as shown in Figure 6. The result indicates that the gasifier mass flow rate increases the amount of hot water production when maintained at 95 °C. This slight increase in gasifier mass flow rate has a negligible impact on ETI, decreasing slightly from 2.115 to 2.109 units. The trend is attributed to the variation in the flue gas temperature after the water heater. Also, similar thermodynamic conditions are responsible for a low comparative variation on the EUI when the gasifier mass flow rate increases. Conversely, increasing the gasifier mass flow rate reduces the overall ESI. The system’s ESI dropped from 0.822 to 0.358, which is attributed to large exergy destruction in the reheater and LPT.

**4.5.6 Effect of ammonia mass fraction on thermo-environmental parameters**

Figure 7 shows the effect of ammonia mass fraction on thermo-environmental parameters. The variations in the ammonia mass fraction slightly affect the ETI, EUI, and ESI. Higher ammonia concentration results in a rich and increased quantity of ammonium vapour for expansion in the turbine and evaporation in the evaporators. Thus, the power output of the Kalina system rises. Nonetheless, since the EUI, ETI, and ESI are wholly affected by the variation of the net output from the entire multigeneration plant, the effect of Kalina output is negligible on these thermo-environmental parameters. However, due to high exergy destruction in the Kalina vapour generator resulting from the increase in the ammonium concentration, the ESI reduces slightly from 0.5279 to 0.5251 between ammonia concentrations of 0.25 and 0.40.

**4.5.7 Effect of primary zone temperature on environmental emissions**

Figure 8 present the effect of the primary zone temperature on the production of CO, CO<sub>2</sub> and NO<sub>x</sub> emissions. The parameters of the primary zone temperature in the combustion chamber were estimated using the methodology in [24].

**Table 7.** Summary of systems component and total exergy destruction

Component	Exergy destruction (ED) [kW]	[%] ED/cycle and component	[%] total of ED
GT CC	49903.00	54.652	46.901
GT HEX	5971.00	6.539	5.612
GT HPC	4692.00	5.139	4.409
GT HPT	2466.00	2.701	2.318
GT INTCL	1481.00	1.621	1.392
GT LPC	4001.00	4.382	3.760
GT LPT	2183.00	2.391	2.052
GT reheater	20613.00	22.575	19.373
GT total ED	91310.00	100.000	85.818
KAL. CND1	219.3.00	15.517	0.206
KAL. CND2	10.480	0.742	0.009
KAL. EVP1	8.568	0.606	0.008
KAL. HEX1	1.813	0.128	0.002
KAL. HEX2	8.265	0.585	0.008
KAL. PUMP1	0.003	0.00018	2.5E-06
KAL. SEP1	49.040	3.469	0.046
KAL. SEP2	2.147	0.151	0.002
KAL. TURB	0.000	0.000	0.000
KAL. VALVE1	84.560	5.983	0.079
KAL. VALVE2	1.301	0.092	0.001
KAL. VALVE3	21.820	1.544	0.021
KAL. VG	1006.00	71.181	0.945
Kalina total ED	1413.290	100.00	1.328
VAS absorber	213.900	21.543	0.201
VAS condenser 2	127.200	12.811	0.119
VAS desorber	318.800	32.108	0.299
VAS evaporator 2	155.100	15.621	0.146
VAS HEX 3	3.942	0.397	0.004
VAS pump 2	0.000	0.000	0.000
VAS valve 4	17.550	1.768	0.016
VAS valve 5	156.400	15.752	0.147
VAS ED	992.890	100.000	0.933
Water heater	12502.00	100.000	11.750
PEM electrolyzer	115.600	63.658	0.109
PEM HEX	65.990	36.338	0.062
PEM oxygen separator	0.0060	0.0032	5.5E-06

The primary zone temperature affects the emission rates at critical temperatures in excess of 1895 °K. The rate of NO<sub>x</sub> emissions are higher (10.57 kg at 2400 °K) compared to CO (0.01380 kg at 2400 °K). Consequently, it is recommended to operate the system at optimum primary zone temperature to reduce NO<sub>x</sub> emissions. The CO<sub>2</sub> emissions from the system are not directly related to the primary zone temperature but to the emissions coefficient of the natural gas after combustion and its mass flow rate. However, this system calculated the instantaneous CO<sub>2</sub> emissions at 27.35 kg/s at a flue gas mass flow rate of 205.5 kg/s.

**Table 8.** Summary of initial investment, monetary flow rate and Levelized capital cost rate

Plant component	Purchase of equipment cost (\$) *	Levelized cost per year (\$/yr.)*	Levelized cost per hour (\$/hr.)*
GT CC	213978	38022	5.038
GT HEX	155098	27559	3.652
GT HPC	517708	91992	12.19
GT HPT	1762604	313198	41.5
GT INTCL	93214	16563	2.195
GT LPC	517708	91992	12.19
GT LPT	1452180	258038	34.19
GT reheater	213093	37864	5.017
KAL. CND1	1953	347	0.04598
KAL. CND2	1953	347	0.04598
KAL. EVP1	1953	347	0.04598
KAL. HEX1	3353	595.9	0.07895
KAL. HEX2	3353	595.9	0.07895
KAL. PUMP1	5405	960.5	0.1273
KAL. SEP1	13067	2322	0.3076
KAL. SEP2	13067	2322	0.3076
KAL. TURB	156801	27862	3.692
KAL. VALVE1	325.5	57.83	0.007663
KAL. VALVE2	325.5	57.83	0.007663
KAL. VALVE3	325.5	57.83	0.007663
KAL. VG	191786	34079	4.515
VAS absorber	1060	188.3	0.02495
VAS condenser 3	1137	202.1	0.02678
VAS desorber	2679	476.1	0.06308
VAS evaporator 2	1017	180.7	0.02395
VAS HEX 3	1254	222.8	0.02952
VAS pump 2	5321	940.3	0.0123
VAS valve 4	325.5	57.83	0.007663
VAS valve 5	325.5	57.83	0.007663
Water heater	2444	434.3	0.05755
PEM electrolyser	3823	679.2	0.0225
PEM HEX	955.6	169.8	0.0225
PEM oxygen separator	1147	203.8	0.027

**4.5.8 Effect of gasifier temperature and mass flow on the unit cost of electricity**

The effect of gasifier temperature and mass flow rate on the unit cost of electricity is shown in Figure 9. The temperature of the gasifier and the mass flow correlate with the unit cost of electricity (UCOE) regarding the system power output. The UCOE based on the initial design conditions was obtained as 21.44 N/kWh (USD 0.0329/kWh), which is more attractive than the current tariff plan in Nigeria of 54 N/kWh (USD 0.083/kWh). The gasifier temperature and the mass flow rate increase leads to a decrease in the UCOE following a high output generation from the system. Therefore, the reduction in UCOE is more with respect to the gasifier temperature increase than the gasifier mass flow rate.

**4.5.9 Effect of ammonium mass fraction on the unit cost of electricity**

The effect of ammonia mass fraction on the UCOE and PEC for the entire system is shown in Figure 10. The increase in ammonia mass fraction leads to a slight increase in the

UCOE. High ammonium mass fraction results in high turbine output, which increases the turbine purchase equipment cost. Although there is an additional power generation from a high ammonium mass fraction, the UCOE increase is negligible.

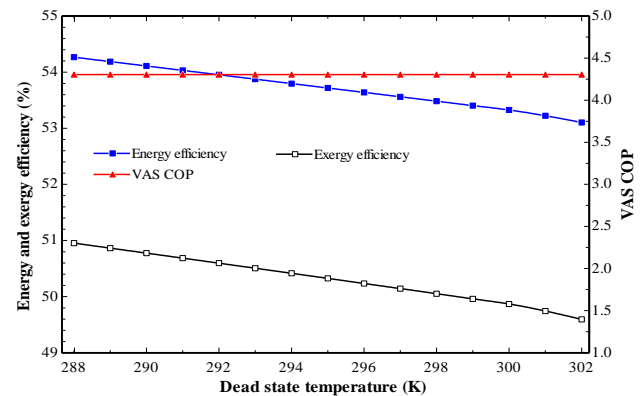


**Figure 2.** Dead state temperature on performance parameters

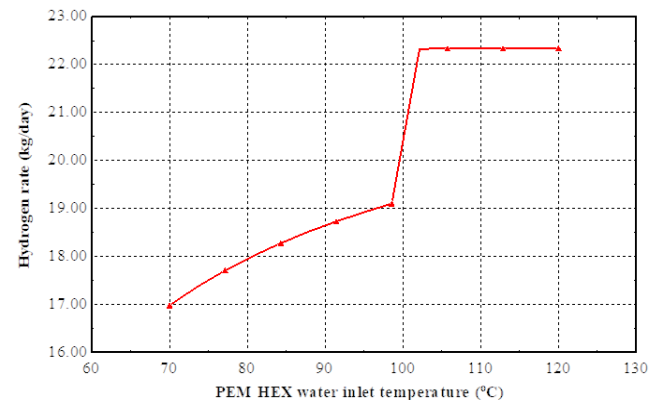


**Figure 3.** Effect of heat input on the PEM electrolyzer heat exchanger

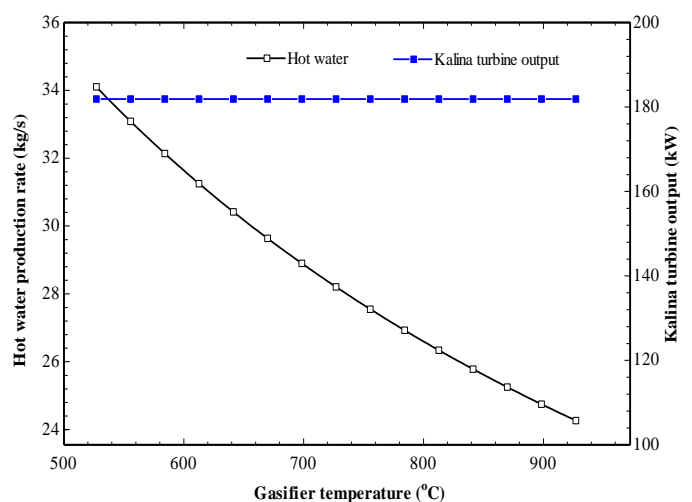


**Figure 4.** Gasifier temperature effect on hot water production rate and power output

**Table 9.** Exergoeconomic parameters for the GT and reheater topping cycle

Component	$\dot{C}_F$ (\$/GJ)	$\dot{C}_P$ (\$/GJ)	$\dot{E}_D$ (MW)	$\dot{C}_D$ (\$/hr.)	Z (\$/hr.)	Z + $\dot{C}_D$ (\$/hr.)	$f_k$ (%)	$r_k$ (%)
GT CC	0.2217	0.3007	49.903	39.8243	5.038	44.8623	11.30	35.63
GT HEX	0.2139	0.3028	5.971	4.597719	3.652	8.2497	44.30	41.55
GT HPC	0.3649	0.6516	4.692	6.165175	12.19	18.355	66.40	78.53
GT HPT	0.3007	0.4851	2.466	2.669287	41.5	44.169	93.40	61.34
GT INTC	0.6967	3.0239	1.481	3.714362	2.195	5.909	37.10	334.06
GT LPC	0.4851	0.6969	4.001	6.986962	12.19	19.177	63.50	43.67
GT LPT	0.2139	0.3930	2.183	1.680655	34.19	35.871	95.30	83.77
GT REH	0.1749	0.2139	20.613	12.98443	5.017	18.001	27.90	22.22

**Table 10.** Exergoeconomic parameters for the Kalina power-cooling bottoming cycle

Component	$\dot{C}_F$ (\$/GJ)	$\dot{C}_P$ (\$/GJ)	$\dot{E}_D$ (MW)	$\dot{C}_D$ (\$/hr.)	Z (\$/hr.)	Z + $\dot{C}_D$ (\$/hr.)	$f_k$ (%)	$r_k$ (%)
KAL. CND1	2.5492	6.1994	0.2193	2.0126	0.0460	2.0585	2.230	143.190
KAL. CND2	2.4799	14.579	0.0105	0.0935	0.0459	0.1395	32.95	487.876
KAL. EVP1	1.0000	2.1805	0.0086	0.0000	0.0459	0.0459	100.00	118.051
KAL. HEX1	1.9857	4.7164	0.0018	0.0130	0.0789	0.0919	85.89	137.515
KAL. HEX2	2.4787	13.327	0.0083	0.0738	0.0789	0.1527	51.70	437.671
KAL. PUM1	8.0153	14.968	2.6E-06	7.5E-05	0.1273	0.1274	99.94	86.738
KAL. SEP1	2.1012	2.3329	0.0490	0.3710	0.3076	0.6786	45.33	11.025
KAL. SEP2	2.3329	2.5496	0.0022	0.0180	0.3076	0.3256	94.46	9.2890
KAL. TURB	2.3326	7.5825	0.0000	0.0000	3.6920	3.6920	100.00	225.064
KAL. VAL1	2.3329	3.9644	0.0846	0.7102	0.0077	0.7179	1.07	69.928
KAL. VAL2	2.5474	4.1527	0.0013	0.0119	0.0077	0.0196	3.91	63.019
KAL. VAL3	2.5542	6.3918	0.0218	0.2006	0.0077	0.2083	3.68	150.247
KAL. VG	0.2129	1.9493	1.0060	0.7713	4.5150	5.2864	85.41	815.217

**Table 11.** Exergoeconomic parameters for the vapor absorption bottoming cycle

Component	$\dot{C}_F$ (\$/GJ)	$\dot{C}_P$ (\$/GJ)	$\dot{E}_D$ (MW)	$\dot{C}_D$ (\$/hr.)	Z (\$/hr.)	Z + $\dot{C}_D$ (\$/hr.)	$f_k$ (%)	$r_k$ (%)
VAS ABS	0.0909	1.2461	0.2139	0.0701	0.0250	0.0950	26.26	1269.62
VAS CON 3	1.4121	4.5304	0.1272	0.6466	0.0268	0.6734	3.980	220.82
VAS DESB	0.8303	1.4123	0.3188	0.9529	0.0631	1.0160	6.210	70.097
VAS evaporator 2	1.0001	1.0224	0.1551	0.0000	0.0240	0.0240	100.00	2.23
VAS HEX 3	0.3313	0.6916	0.0039	0.0047	0.0296	0.0342	86.26	108.76
VAS pump 2	15.014	17.473	0.0000	0.0000	1.02E-07	1.02E-07	100.00	16.38
VAS valve 4	0.1408	0.3406	0.0176	0.0089	0.0077	0.01660	46.28	141.91
VAS valve 5	20.663	24.9180	0.0031	0.2290	0.0050	0.2340	97.69	20.59

**Table 12.** Exergoeconomic parameters for the PEM electrolyzer

Component	$\dot{C}_F$ (\$/GJ)	$\dot{C}_P$ (\$/GJ)	$\dot{E}_D$ (MW)	$\dot{C}_D$ (\$/hr.)	Z (\$/hr.)	Z + $\dot{C}_D$ (\$/hr.)	$f_k$ (%)	$r_k$ (%)
WATER heater	0.2140	1.2793	12.502	9.6297	0.05755	9.6873	5.9	497.93
PEM Electrolyzer	4.5650	9.3813	0.116	1.8998	0.0225	1.9223	1.17	105.50
PEM HEX	6.3660	6.7198	0.066	1.5124	0.0225	1.5348	1.47	5.56
PEM oxygen separator	9.3813	9.4491	5.79E-06	0.0002	0.0270	0.027196	99.28	0.723

**4.5.10 Effect of gasifier temperature and mass flow on system total cost**

In Figure 11, the effect of gasifier mass flow rate and temperature is investigated on the system's total cost. The system's net cost was estimated at \$ 5335411.5 based on the operating conditions in Table 6. The total cost comprises purchasing equipment (PEC) for all system components. Thus an increase in both the gasifier temperature and mass flow rate significantly raises the total PEC of the system.

The resultant effect of increased gasifier temperature and mass flow rate cumulatively enhances the power requirements of the LPT. Consequently, the PEC of the LPT, GT HEX, Kalina vapour generator, and water heater contributes about 33.76 % of the entire plant's PEC.

**4.6 Optimum parameters**

For optimal performance, the study considered the following objective functions (OBF): total exergy efficiency

( $\psi$ ) and the total product cost rate. The  $\psi$  is to be maximized, while the total cost rate is to be reduced or maximized. The total cost rate model equation of the multigeneration plant is integrated with the cost rate of the pollution damage.

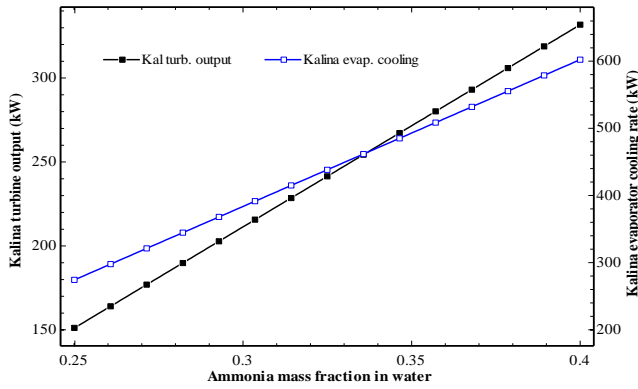


Figure 5. Effect of ammonia mass fraction on Kalina cycle performance

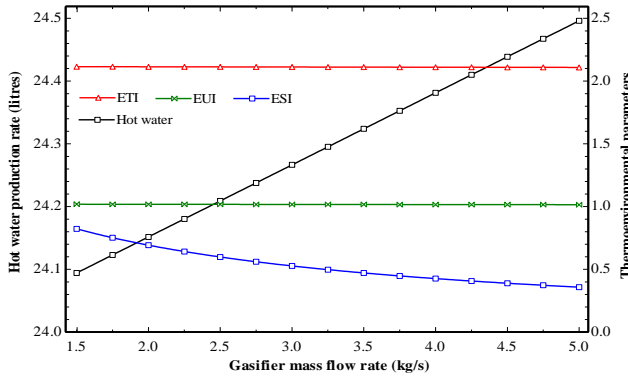


Figure 6. Gasifier mass flow rate on environmental parameters and hot water production rate

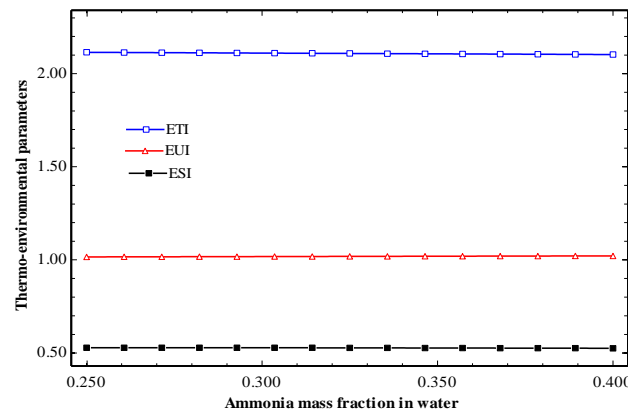


Figure 7. Effect of ammonia mass fraction on thermo environmental parameter

The OBFs are described as follows:

$$\psi_{overall} = \frac{\dot{E}_{W_{LPT}} + \dot{E}_{W_{HPT}} + \dot{E}_{W_{KT}} + \dot{E}_{R_{Kalina}} + \dot{E}_{R_{VAS}}}{A_d} - \left\{ \dot{E}_{W_{LPC}} + \dot{E}_{W_{HPC}} + \sum_{i=1}^6 \dot{E}_{W_{P_i}} \right\} \quad (26)$$

Where  $A_d$  of Eq (26) is expressed in Eq (27).

$$A_d = \left\| \left[ 1 - \frac{T_0}{T_6} \right] \dot{Q}_6 + \left[ 1 - \frac{T_0}{T_9} \right] \dot{Q}_9 \right\| \quad (27)$$

Where  $\dot{Q}_6$  and  $\dot{Q}_9$  are the heat addition into the GT combustion chamber and the complementary firing process (the reheater) Figure 1.

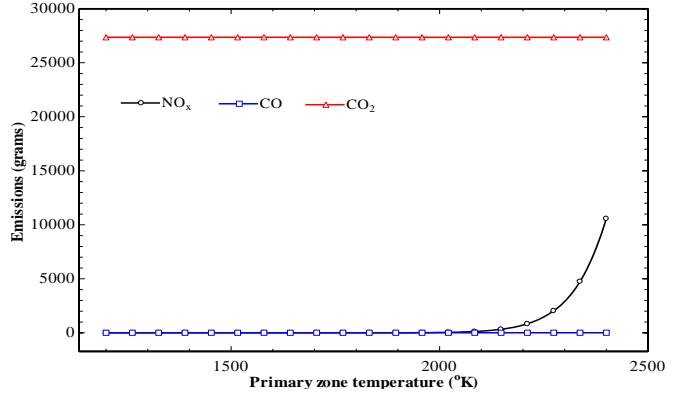


Figure 8. Effect of primary zone temperature on environmental emissions

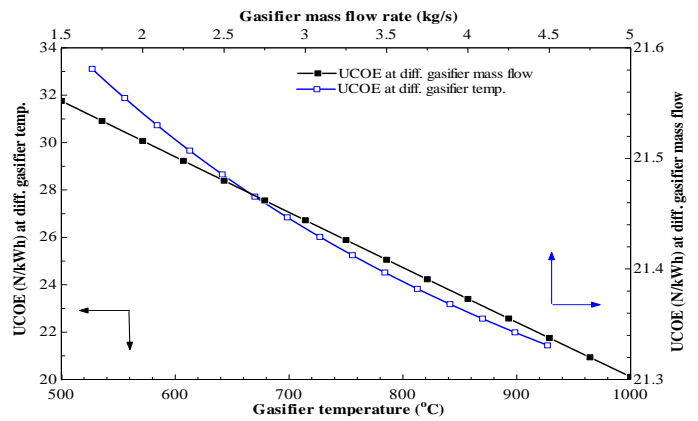


Figure 9. Effect of gasifier temperature and mass flow on the unit cost of electricity

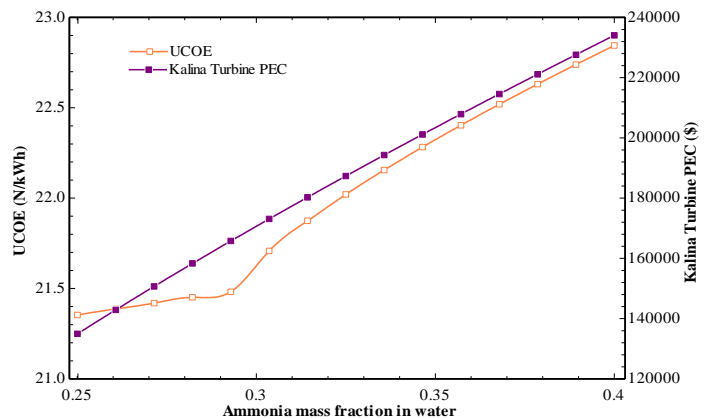


Figure 10. Effect of ammonia mass fraction on the unit cost of electricity

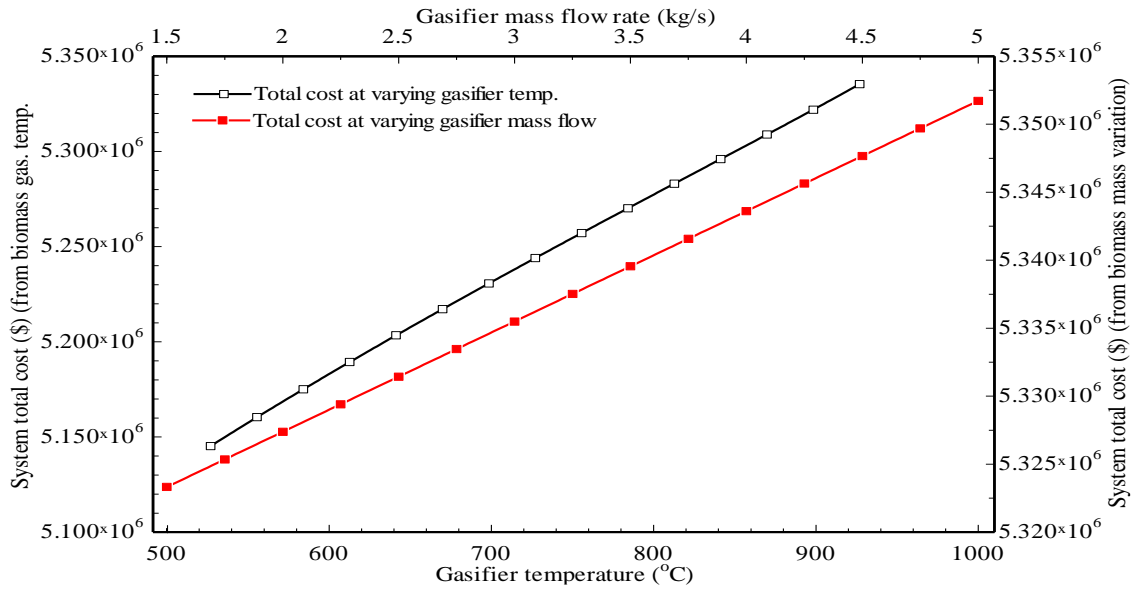


Figure 11. Effect of gasifier temperature and mass flow on system total cost

Table 13. Components of optimization functions and parameters

Performance index	Optimization function	Decision variables	Optimization constraints
$W_{LPC}$	$\dot{m}_1 c_p \frac{T_1}{\eta_{LPC}} [(r_p)^k - 1]$	$\eta_{LPC}, r_p$	$0.80 \leq LPC \leq 0.90$
$W_{HPC}$	$\dot{m}_3 c_p \frac{T_3}{\eta_{HPC}} [(r_p)^k - 1]$	$\eta_{LPC}, r_p$	$0.80 \leq LPC \leq 0.90$
$W_{LPT}$	$\dot{m}_{10} c_p T_{10} \eta_{LPT} \left  1 - \frac{1}{(r_p)^k} \right $	$\eta_{LPC}, r_p, T_{10}$	$0.80 \leq LPC \leq 0.9$ $8 \leq r_p \leq 16, 1150 \leq T_{10} \leq 1250$
$W_{HPT}$	$\dot{m}_7 c_p T_7 \eta_{HPT} \left  1 - \frac{1}{(r_p)^k} \right $	$\eta_{LPC}, r_p, T_7$	$0.80 \leq LPC \leq 0.9, 8 \leq r_p \leq 16, 1150 \leq T_7 \leq 1250 K$
$W_{Kal.Turb}$	$\dot{m}_{28}  h_{28} - h_{29}  +  \dot{m}_{28} - \dot{m}_{29}   h_{29} - h_{33} $	$P_{28}$ , pressure at $T_{28}, h_{28}$	$435 \leq T_{28} \leq 439 K$
$Q_{EVP1}$	$\dot{m}_{30}  h_{31} - h_{32} $	$T_{30}$	$T_{61}, -3 \text{ and } -1.5^\circ C$
$VP_{generator}$	$\dot{m}_{12}  h_{12} - h_{13} $	$T_{12}$	$270 \leq T_{60} \leq 282$
$Q_{EVP2}$	$\dot{m}_{40}  h_{41} - h_{40} $	$T_{40}$	$T_{44}, -5.8 \text{ and } -1.5^\circ C$
$\dot{C}_{ost, Total}$	$\dot{C}_{fuel} + \dot{C}_{env.} + \sum_k \dot{Z}_k$	Described parameters	

The total cost rate of the system and the cost rate due to environmental impact are presented in Eqs (28) and (29). The components of the optimization function, objective functions, constraints and key performance indices are depicted in Table 13.

$$\dot{C}_{Tot} = \dot{C}_{fuel} + \dot{C}_{env.} + \sum_k \dot{Z}_k \tag{28}$$

$$\dot{C}_{env} = C_{NO_x} \dot{m}_{NO_x} + C_{CO_2} \dot{m}_{CO_2} + C_{CO} \dot{m}_{CO} \tag{29}$$

Where the unit damage costs  $C_{NO_x}$ ,  $C_{CO_2}$  and  $C_{CO}$  are taken as 0.02186 \$/kg, 6.863\$/kg and 0.023 \$/kg, respectively.

The GA (genetic algorithm) was applied in the optimization due to its flexibility in simplifying multi-variable and multi-objective problems. In this analysis, Ninety groups of the Pareto-frontiers from the GA were described following the OBFs and the equivalent constraints. The 17th Pareto-front correspond to the optimum ( $\psi$ ) and minimum cost rate calculated at 45.32 % and 125.84 \$/hr, separately. The corresponding parameters occur at a compression ratio (CR) of 8, with isentropic efficiencies of LPC, HPC, LPT, and HPT existing at 88%. Also, the intercooler exit temperature and the inlet temperature to the combustion chamber and reheater were calculated at 386.7K, 1140 K and 1240.3 K. The optimal

inlet pressures of the Kalina system were obtained at 20 kPa. The specific emissions rate at the optimum operating conditions are calculated at 123.34, 2.87E-07 and 0.214 kg/MWh for CO<sub>2</sub>, CO and NO<sub>x</sub>, respectively. The improvement potential of the environmental discharges is for CO<sub>2</sub>, 1.56 %, NO<sub>x</sub>, 4.33 % and CO, 3.65 %, with optimum hydrogen production.

**5. Conclusion**

A Kalina-based multigeneration cycle with increased heat addition to the PEM electrolyzer for hydrogen and water production was performed. The results are summarised as follows: The multigeneration energy system has a net energy and exergy efficiency of 53.48 and 50.05 %, respectively. Additionally, the system has improved topping cycle efficiency by 19.03 and 2.58 %, respectively, from the original values of 34.45 and 47.47 %. At the cycle level, the gas turbine contributed up to 85.81 % of the ED. The combustion chamber and reheater contributed about 54.65 and 22.57 % of the total ED destructions. The system overall exergo-thermal index (ETI) stood at 1.713 with the gas turbine system alone the ETI was obtained as 2.106, which suggests a higher thermal impact on the environment without the addition of the lower cycles. The system has a hydrogen production rate of 0.1524 kg/h with cooling rate and COP calculated at 3498 kW and 4.304 respectively. The ESI for the system was relatively low, with a value of 0.5242. The low ESI arises from the large ED in the topping cycle, which contributed about 66 % of total system ED. The exergoeconomic result indicates a low average cost of energy from the gas turbine (0.836 \$/GJ) compared to the Kalina subsystem (6.53 \$/GJ) and vapour absorption system (3.24 \$/GJ).

**Ethical issue**

The authors are aware of and comply with best practices in publication ethics, specifically with regard to authorship (avoidance of guest authorship), dual submission, manipulation of figures, competing interests, and compliance with policies on research ethics. The author adheres to publication requirements that the submitted work is original and has not been published elsewhere.

**Data availability statement**

Datasets analyzed during the current study are available and can be given following a reasonable request from the corresponding author.

**Conflict of interest**

The authors declare no potential conflict of interest.

**References**

[1] M. Azam .Energy and economic growth in developing Asian economies, J. of the Asia Pacific Econo. 25 (3) (2020) 447-471 DOI: 10.1080/13547860.2019.1665328

[2] C. Cicea., C. N Ciocoiu., C. Marinescu. (2021). Exploring the Research Regarding Energy–Economic Growth Relationship. *Energies* 14(9) (2021) 2661. Doi: 10.3390/en14092661.

[3] N. Dev, R. Attri. Performance analysis of combined cycle power plant. *Front in Energy*, 9(4) (2015) 371-386.

[4] E. Bellos., C. Tzivanidis. Optimization of a solar-driven trigeneration system with nanofluids-based

parabolic trough collectors. *Energies*10 (2017) 848-877

[5] G. Manente, G. (2016). High performance integrated solar combined cycles with minimum modifications to the combined cycle power plant design. *Energy Convers. Manag.* 111 (2016)186–97.

[6] C. Stefano., D. Micheli., M. Reini., R. Tacconi. (2013). Bottoming organic Rankine cycle for a small scale gas turbine: A comparison of different solutions. *Applied Energy*, 106 (2013) 355-364. doi:10.1016/j.apenergy.2013.02.004.

[7] B.Peris., J.Navarro-Esbrí., F. Molés. Bottoming organic Rankine cycle configurations to increase Internal Combustion Engines power output from cooling water waste heat recovery. *Applied Therm. Eng.* 61(2) (2013). 364-371.

[8] F. I. Abam., E. B. Ekwe, S. O. Effiom. C. Afangideh. Performance and thermo- sustainability analysis of non-hybrid organic Rankine cycles (ORCs) at varying heat source and evaporator conditions. *Australian J. Mechanical Eng.* 16 (3) (2018) 238-248

[9] H. Gao., F. Chen. Thermo-Economic Analysis of a Bottoming Kalina Cycle for Internal Combustion Engine Exhaust Heat Recovery. *Energies*, 11(11) 2018 3044 doi: 10.3390/en11113044.

[10] L. A. Prananto., I. N. Zaini., B.I. Mahendranata., F. B. Juangsa, F Bagja; M. Aziz, T. Soelaiman., A. Fauzi (2018). Use of the Kalina cycle as a bottoming cycle in a geothermal power plant: Case study of the Wayang Windu geothermal power plant. *Appl. Thermal Eng.* 132, (2018) 686-696.

[11] G. Guzmán., L. D, L Reyes, E. Noriega., H. Ramírez., Bula., A. Fontalvo. Thermal Optimization of a Dual Pressure Goswami Cycle for Low Grade Thermal Sources. *Entropy* 21, (2019)711; doi:10.3390/e21070711

[12] Dev, N. and Attri, R. (2015). Performance analysis of combined cycle power plant. *Frontiers in Energy*, 9(4): 371–386.

[13] Ahmadi, Pouria; Dincer, Ibrahim; Rosen, Marc A. (2012). Exergo-environmental analysis of an integrated organic Rankine cycle for trigeneration. *Energy Conversion and Management*, 64(), 447–453. doi:10.1016/j.enconman.2012.06.001.

[14] Sharifishourabi, M., Ratlamwala, T., Alimoradiyan, H. and Sadeghizadeh, E. (2016). Performance assessment of a multigeneration system based on organic Rankine cycle. *Iranian Journal of Science and Technology, Transactions of Mechanical Engineering* 3: 225-232.

[15] F. I. Abam, O. E. Diemuodeke, E. B. Ekwe, M. Alghassab, O. D. Samuel, Z. A. Khan, M. Imran, M. Farooq. Exergoeconomic and Environmental Modeling of Integrated Polygeneration Power Plant with Biomass-Based Syngas Supplemental Firing. *Energies* 2020, 13, 6018

[16] Anvari, S., Mahian, O., Taghavifar, H., Wongwises, S., and Desideri, U. (2020). 4E analysis of a modified multi-generationsystem designed for power,

- heating/cooling, and water desalination. *Applied Energy*, 270, 115107.
- [17] Chitgar, Nazanin; Moghimi, Mahdi (2020). Design and evaluation of a novel multi-generationsystem based on SOFC-GT for power, desalinated water and hydrogen supply. *Energy*, 117162-. doi:10.1016/j.energy.2020.117162.
- [18] Khalid, F., Dincer, I., & Rosen, M. A. (2017). Techno-economic assessment of a solar-geothermal multi-generationsystem for buildings. *International Journal of Hydrogen Energy*, 1-9. doi:http://dx.doi.org/10.1016/j.ijhydene.2017.03.185.
- [19] Cao, L., Lou, J., Wang, J., & Dai, Y. (2018). Exergy analysis and optimization of a combined cooling and power system driven by geothermal energy for ice-making and hydrogen production. *Energy Conversion and Management*, 174, 886-896. <https://doi.org/10.1016/j.enconman.2018.08.067>.
- [20] F. I. Abam, T. A. Briggs, E. B. Ekwe, C. G. Kanu, Samuel O. Effiom, M. C. Ndukwu, S. O. Ohunakin, M. I. Ofem (2018): Exergy analysis of a novel low-heat recovery organic Rankine cycle (ORC) for combined cooling and power generation, *Energy Sources, Part A: Recovery, Utilization, and Environmental Effects*, DOI: 10.1080/15567036.2018.1549140
- [21] Roy, D. and Ghosh, R. (2017). Energy and exergy analyses of an integrated biomass gasification combined cycle employing solid oxide fuel cell and organic Rankine cycle, *Clean Techn Environ Policy* DOI 10.1007/s10098-017-1358-5.
- [22] Chitsaz, A., Mehr, A. S., Mahmoudi, S. M. (2015). Exergoeconomic analysis of a trigeneration system driven by a solid oxide fuel cell. *Energy conversion and management*, 106:921-31.
- [23] K. Owebor, C. O. C. Oko, E. O. Diemuodeke und O. J. Ogorure, „Thermo- environmental and economic analysis of an integrated municipal waste-to-energy solid oxide fuel cell, gas-steam- organic fluid-and absorption refrigeration cycle thermal power plants,“ *Applied Energy*, Bd. 239, pp. 1385-1401, 2019.
- [24] O. L. Gulder. Flame temperature estimation of conventional and future jet fuels, *Journal of Engineering for Gas Turbines and Power*, Bd. 108, Nr. (2), pp. 376-380, 1986.
- [25] Aydin, H. (2013). Exergetic sustainability analysis of LM 6000 gas turbine power plant with steam cycle. *Energy* 57: 766-774.



This article is an open-access article distributed under the terms and conditions of the Creative Commons Attribution (CC BY) license (<https://creativecommons.org/licenses/by/4.0/>).

Appendix

Table 1. Summary of the energy and exergy balances, as well as the exergy of fuel and product for the system

Component	Energy Balance	Exergy Balance	Exergy of Fuel	Exergy of Product
GT LPC	$\dot{m}_1 h_1 + \dot{W}_{LPC} = \dot{m}_2 h_2$	$\dot{E}_1 + \dot{W}_{LPC} = \dot{E}_2 + \dot{E}_{D,LPC}$	$\dot{W}_{LPC}$	$\dot{E}_2 - \dot{E}_1$
GT intercooler	$\dot{m}_2 h_2 + \dot{m}_{48} h_{48} = \dot{m}_3 h_3 + \dot{m}_{49} h_{49}$	$\dot{E}_2 + \dot{E}_{48} = \dot{E}_3 + \dot{E}_{49} + \dot{E}_{D,INT}$	$\dot{E}_2 - \dot{E}_3$	$\dot{E}_{49} - \dot{E}_{48}$
GT HPC	$\dot{m}_3 h_3 + \dot{W}_{HPC} = \dot{m}_4 h_4$	$\dot{E}_3 + \dot{W}_{LPC} = \dot{E}_4 + \dot{E}_{D,HPC}$	$\dot{W}_{HPC}$	$\dot{E}_4 - \dot{E}_3$
GT Hex	$\dot{m}_4 h_4 + \dot{m}_{11} h_{11} = \dot{m}_5 h_5 + \dot{m}_{12} h_{12}$	$\dot{E}_4 + \dot{E}_{11} = \dot{E}_5 + \dot{E}_{12} + \dot{E}_{D,GT\ HEX}$	$\dot{E}_{11} - \dot{E}_{12}$	$\dot{E}_5 - \dot{E}_4$
GT CC	$\dot{m}_6  LHV_6  + \dot{m}_5 h_5 = \dot{m}_7 h_7$	$\dot{E}_5 + \dot{E}_6 = \dot{E}_7 + \dot{E}_{D,GT\ CC}$	$\dot{E}_5 + \dot{E}_6$	$\dot{E}_7$
GT HPT	$\dot{m}_7 h_7 = \dot{m}_8 h_8 + \dot{W}_{HPT}$	$\dot{E}_7 = \dot{E}_8 + \dot{W}_{HPC} + \dot{W}_{LPC} + \dot{E}_{D,HPT}$	$\dot{E}_7 - \dot{E}_8$	$\dot{W}_{HPC} + \dot{W}_{LPC}$
GT REH	$\dot{m}_9  LHV_9  + \dot{m}_8 h_8 = \dot{m}_{10} h_{10}$	$\dot{E}_8 + \dot{E}_9 = \dot{E}_{10} + \dot{E}_{D,GT\ REH}$	$\dot{E}_8 + \dot{E}_9$	$\dot{E}_{10}$
GT LPT	$\dot{m}_{10} h_{10} = \dot{m}_{11} h_{11} + \dot{W}_{LPT}$	$\dot{E}_{10} = \dot{E}_{11} + \dot{W}_{LPT} + \dot{E}_{D,LPT}$	$\dot{E}_{10} - \dot{E}_{11}$	$\dot{W}_{LPT}$
Kal. Vap Gen.	$\dot{m}_{12} h_{12} + \dot{m}_{37} h_{37} = \dot{m}_{13} h_{13} + \dot{m}_{17} h_{17}$	$\dot{E}_{12} + \dot{E}_{37} = \dot{E}_{13} + \dot{E}_{17} + \dot{E}_{D,VapGen}$	$\dot{E}_{12} - \dot{E}_{13}$	$\dot{E}_{17} - \dot{E}_{37}$
Kal. Sep 1	$\dot{m}_{17} h_{17} = \dot{m}_{18} h_{18} + \dot{m}_{22} h_{22}$	$\dot{E}_{17} = \dot{E}_{18} + \dot{E}_{22} + \dot{E}_{D,Kal\ S1}$	$\dot{E}_{17}$	$\dot{E}_{18} + \dot{E}_{22}$
Kal. Valve 1	$\dot{m}_{22} h_{22} = \dot{m}_{23} h_{23}$	$\dot{E}_{22} = \dot{E}_{23} + \dot{E}_{D,Kal\ V1}$	$\dot{E}_{22}$	$\dot{E}_{23}$
Kal. Valve 2	$\dot{m}_{21} h_{21} = \dot{m}_{24} h_{24}$	$\dot{E}_{21} = \dot{E}_{24} + \dot{E}_{D,Kal\ V2}$	$\dot{E}_{21}$	$\dot{E}_{24}$
Kal. Turb.	$\dot{m}_{18} h_{18} = \dot{m}_{20} h_{20} + \dot{m}_{18} W_{TKal} + \dot{m}_{34} W_{P1} + \dot{m}_{42} W_{P2}$	$\dot{E}_{18} = \dot{E}_{20} + \dot{E}_{WTKal} + \dot{E}_{WP1} + \dot{E}_{WP2} + \dot{E}_{DTKal}$	$\dot{E}_{18} - \dot{E}_{20}$	$\dot{E}_{WTKal} + \dot{E}_{WP1} + \dot{E}_{WP2}$
Kal. Sep 2	$\dot{m}_{20} h_{20} = \dot{m}_{28} h_{28} + \dot{m}_{21} h_{21}$	$\dot{E}_{20} = \dot{E}_{28} + \dot{E}_{21} + \dot{E}_{D,Kal\ S2}$	$\dot{E}_{20}$	$\dot{E}_{28} + \dot{E}_{21}$
Kal. CND 1	$\dot{m}_{28} h_{28} + \dot{m}_{59} h_{59} = \dot{m}_{29} h_{29} + \dot{m}_{60} h_{60}$	$\dot{E}_{28} + \dot{E}_{59} = \dot{E}_{29} + \dot{E}_{60} + \dot{E}_{D,CND1}$	$\dot{E}_{28} - \dot{E}_{29}$	$\dot{E}_{60} - \dot{E}_{59}$
Kal. Valve 3	$\dot{m}_{28} h_{28} = \dot{m}_{29} h_{29}$	$\dot{E}_{28} = \dot{E}_{29} + \dot{E}_{D,Kal\ V3}$	$\dot{E}_{28}$	$\dot{E}_{29}$
Kal. Evap 1	$\dot{m}_{12} h_{12} + \dot{m}_{37} h_{37} = \dot{m}_{13} h_{13} + \dot{m}_{17} h_{17}$	$\dot{E}_{12} + \dot{E}_{37} = \dot{E}_{13} + \dot{E}_{17} + \dot{E}_{D,V.GEN}$	$\dot{E}_{12} - \dot{E}_{13}$	$\dot{E}_{17} - \dot{E}_{37}$
Kal. HEX 1	$\dot{m}_{26} h_{26} + \dot{m}_{36} h_{36} = \dot{m}_{27} h_{27} + \dot{m}_{37} h_{37}$	$\dot{E}_{26} + \dot{E}_{36} = \dot{E}_{27} + \dot{E}_{37} + \dot{E}_{D,Kal\ HEX1}$	$\dot{E}_{26} - \dot{E}_{27}$	$\dot{E}_{37} - \dot{E}_{36}$
Kal. HEX 2	$\dot{m}_{32} h_{32} + \dot{m}_{35} h_{35} = \dot{m}_{33} h_{33} + \dot{m}_{36} h_{36}$	$\dot{E}_{32} + \dot{E}_{35} = \dot{E}_{33} + \dot{E}_{36} + \dot{E}_{D,Kal\ HEX2}$	$\dot{E}_{32} - \dot{E}_{33}$	$\dot{E}_{36} - \dot{E}_{35}$
Kal. CND 2	$\dot{m}_{33} h_{33} + \dot{m}_{57} h_{57} = \dot{m}_{34} h_{34} + \dot{m}_{58} h_{58}$	$\dot{E}_{33} + \dot{E}_{57} = \dot{E}_{34} + \dot{E}_{58} + \dot{E}_{D,KAL\ CND2}$	$\dot{E}_{33} - \dot{E}_{34}$	$\dot{E}_{58} - \dot{E}_{57}$
Kal. Pump 1	$\dot{m}_{34} h_{34} + \dot{m}_{34} W_{P1} = \dot{m}_{35} h_{35}$	$\dot{E}_{34} + \dot{E}_{WP1} = \dot{E}_{35} + \dot{E}_{D,P1}$	$\dot{E}_{WP1}$	$\dot{E}_{35} - \dot{E}_{34}$
VAS desorber	$\dot{m}_{25} h_{25} + \dot{m}_{44} h_{44} = \dot{m}_{26} h_{26} + \dot{m}_{38} h_{38} + \dot{m}_{45} h_{45}$	$\dot{E}_{25} + \dot{E}_{44} = \dot{E}_{26} + \dot{E}_{38} + \dot{E}_{45} + \dot{E}_{D,DESB}$	$\dot{E}_{25} - \dot{E}_{26} + \dot{E}_{44}$	$\dot{E}_{38} - \dot{E}_{45}$
VAS HEX 3	$\dot{m}_{43} h_{43} + \dot{m}_{45} h_{45} = \dot{m}_{44} h_{44} + \dot{m}_{46} h_{46}$	$\dot{E}_{43} + \dot{E}_{45} = \dot{E}_{44} + \dot{E}_{46} + \dot{E}_{D,VAS\ HEX3}$	$\dot{E}_{45} - \dot{E}_{46}$	$\dot{E}_{44} - \dot{E}_{43}$
VAS Valve 5	$\dot{m}_{46} h_{46} = \dot{m}_{47} h_{47}$	$\dot{E}_{46} = \dot{E}_{47} + \dot{E}_{D,VAS\ V5}$	$\dot{E}_{46}$	$\dot{E}_{47}$
VAS Pump 2	$\dot{m}_{42} h_{42} + \dot{m}_{42} W_{P2} = \dot{m}_{43} h_{43}$	$\dot{E}_{42} + \dot{E}_{WP2} = \dot{E}_{43} + \dot{E}_{D,P2}$	$\dot{E}_{WP2}$	$\dot{E}_{43} - \dot{E}_{42}$
VAS Absorber	$\dot{m}_{41} h_{41} + \dot{m}_{47} h_{47} + \dot{m}_{65} h_{65} = \dot{m}_{42} h_{42} + \dot{m}_{66} h_{66}$	$\dot{E}_{41} + \dot{E}_{47} + \dot{E}_{65} = \dot{E}_{42} + \dot{E}_{66} + \dot{E}_{D,ABSB}$	$\dot{E}_{41} + \dot{E}_{47}$	$\dot{E}_{66} - \dot{E}_{65} + \dot{E}_{42}$
VAS EVP 2	$\dot{m}_{40} h_{40} + \dot{m}_{63} h_{63} = \dot{m}_{41} h_{41} + \dot{m}_{64} h_{64}$	$\dot{E}_{40} + \dot{E}_{63} = \dot{E}_{41} + \dot{E}_{64} + \dot{E}_{D,VAS\ EVP2}$	$\dot{E}_{63} - \dot{E}_{64}$	$\dot{E}_{41} - \dot{E}_{40}$
VAS Valve 4	$\dot{m}_{39} h_{39} = \dot{m}_{40} h_{40}$	$\dot{E}_{39} = \dot{E}_{40} + \dot{E}_{D,VAS\ V4}$	$\dot{E}_{39}$	$\dot{E}_{40}$
VAS CND 3	$\dot{m}_{38} h_{38} + \dot{m}_{61} h_{61} = \dot{m}_{39} h_{39} + \dot{m}_{62} h_{62}$	$\dot{E}_{38} + \dot{E}_{61} = \dot{E}_{39} + \dot{E}_{62} + \dot{E}_{D,VAS\ CND3}$	$\dot{E}_{38} - \dot{E}_{39}$	$\dot{E}_{62} - \dot{E}_{61}$
Water heater	$\dot{m}_{13} h_{13} + \dot{m}_{15} h_{15} = \dot{m}_{14} h_{14} + \dot{m}_{16} h_{16}$	$\dot{E}_{13} + \dot{E}_{15} = \dot{E}_{14} + \dot{E}_{16} + \dot{E}_{D,HEATER}$	$\dot{E}_{13} - \dot{E}_{14}$	$\dot{E}_{16} - \dot{E}_{15}$
PEM Electr.	$\dot{m}_{52} h_{52} + \dot{m}_{19} h_{19} = \dot{m}_{53} h_{53} + \dot{m}_{54} h_{54}$	$\dot{E}_{52} + \dot{E}_{19} = \dot{E}_{53} + \dot{E}_{54} + \dot{E}_{D,Electrolyser}$	$\dot{E}_{52} + \dot{E}_{19}$	$\dot{E}_{53} + \dot{E}_{54}$
PEM HEX	$\dot{m}_{58} h_{58} + \dot{m}_{60} h_{60} + \dot{m}_{50} h_{50} = \dot{m}_{51} h_{51} + \dot{m}_{69} h_{69}$	$\dot{E}_{58} + \dot{E}_{60} + \dot{E}_{50} = \dot{E}_{51} + \dot{E}_{69} + \dot{E}_{D,PEM\ HEX}$	$\dot{E}_{58} + \dot{E}_{60} - \dot{E}_{69}$	$\dot{E}_{51} - \dot{E}_{50}$
PEM O <sub>2</sub> separator	$\dot{m}_{54} h_{54} = \dot{m}_{55} h_{55} + \dot{m}_{56} h_{56}$	$\dot{E}_{54} = \dot{E}_{55} + \dot{E}_{56} + \dot{E}_{D,Oxy.sep}$	$\dot{E}_{54}$	$\dot{E}_{55} + \dot{E}_{56}$